



# Multipoint fluorescence correlation spectroscopy using spatial light modulator

JOHTARO YAMAMOTO,<sup>1,2</sup> SHINTARO MIKUNI,<sup>2</sup> AND MASATAKA KINJO<sup>2,\*</sup>

<sup>1</sup>Biomedical Research Institute, National Institute of Advanced Industrial Science and Technology (AIST), Central 6, Higashi 1-1-1, Tsukuba, Ibaraki, 305-8568, Japan

<sup>2</sup>Faculty of Advanced Life Science, Hokkaido University, Kita-21 Nishi-11 Kita-ku, Sapporo, Hokkaido, 001-0021, Japan

\*kinjo@sci.hokudai.ac.jp

**Abstract:** A multipoint holographic fluorescence correlation spectroscopy (MP-hFCS) was successfully developed. The validity of the MP-hFCS was demonstrated using diffusion measurements of fluorescent dye solutions and of fluorescent proteins in single cells. Furthermore, the successful detection of the nuclear transport of a green fluorescent protein-tagged glucocorticoid receptor  $\alpha$  indicates the possibility of being able to monitor directional molecular transport using the MP-hFCS. This allows multipoint analysis of the intermolecular interactions and molecular transport in living cells. Finally, the MP-hFCS can achieve multipoint diffusion measurements with high spatial and time resolution while maintaining a high photon detection sensitivity.

© 2018 Optical Society of America under the terms of the [OSA Open Access Publishing Agreement](#)

## 1. Introduction

Fluorescence correlation spectroscopy (FCS) [1,2] is a powerful tool for measuring the dynamics of fluorescent molecules either in solution or in a living cell. For a living cell, fluorescence measurement that is non-invasive or induces little damage to the cell can be achieved. FCS can reveal the diffusion coefficient, the target molecule concentration, and the brightness of a single molecule. These parameters allow estimations of the molecular size [3], the molecular shape [4,5], the affinities of molecular interactions [6,7], and the degree of homo-multimerization [6]. However, one drawback is that measurements are generally limited to a single point because of the nature of the confocal detection system, despite the fact that different diffusion processes may be ongoing in different cellular compartments under different physiological conditions. To overcome this disadvantage, numerous multipoint diffusion measurement systems have been developed, such as the two-beam cross-correlation method for FCS [8], single plane illumination microscopy based FCS (SPIM-FCS) [9], massively parallel FCS (mpFCS) [10], multipoint total internal reflection (M-TIR-FCS) [11], temporal image correlation spectroscopy (TICS) [12], imaging FCS [13], pair correlation functions (pCFs) [14], and raster image correlation spectroscopy (RICS) [15]. Flow velocity measurement via FCS was first demonstrated using the two-beam cross-correlation method. A single excitation laser beam was separated into two beams using a beam splitter, and the fluorescence emitted from two focal spots was collected using two independent multimode fibers. However, this method is not amenable to increasing the number of measurement points, because of the illumination optics. In contrast, SPIM-FCS, mpFCS, and other camera-based FCS methods [16] can achieve over 1,000 measurement points. However, because of the use of an imaging sensor, either the time resolution or the photon detection sensitivity—or both—must be sacrificed, although only electron multiplying CCD (EM-CCD) has a higher quantum efficiency than the single photodetectors used for FCS, such as the photomultiplier tube (PMT) and the avalanche photodiode. In the future, the time resolution and photon detection sensitivity may reach the current performance of single photodetectors. TICS and scanning FCS, including pCFs, are image processing methods

based on laser scanning microscopy (LSM). They have the advantage that the number of measurement points can be selected up to the maximum pixel number. On the other hand, the time resolution of such methods is limited to the frame rate or the pixel dwell time of the LSM images. RICS is also an image processing method using LSM images. Spatiotemporal information about the target molecule can be extracted from the auto-correlation image of the region of interest (ROI) in the original LSM image. Diffusion information can only be obtained from one ROI; therefore, the spatial resolution is decreased to the size of the ROI. Thus, most multipoint measurement methods for diffusion sacrifice the number of measurement points, spatial resolution, time resolution, and/or photon detection sensitivity. The M-TIR-FCS technique that we previously developed achieved simultaneous measurement at seven two-dimensionally distributed points; however, its measurement points were restricted to the near field of the coverslip.

The multipoint holographic FCS (MP-hFCS) system that we introduce here is an expansion of the two-beam cross-correlation method and M-TIR-FCS that overcomes the limitation of the number of measurement points. The system simultaneously measures seven points distributed in an arbitrary plane at an arbitrary depth in a living cell while maintaining the high spatial resolution and high time resolution of single-point FCS. The number of excitation beam spots can be flexibly increased using a holography technique. The fluorescence emitted from each excitation beam spot is detected by an independent PMT. Practically, the number of measurement points can be increased by increasing the number of detectors.

## 2. Materials and methods

### 2.1 Experimental setup

A schematic of the MP-hFCS system is shown in Fig. 1(a). The laser beam—a 488-nm semiconductor laser (Sapphire 488-20, Coherent, USA)—is expanded and incident to a liquid crystal on a silicon spatial light modulator (SLM, SLM-X02-T, Hamamatsu Photonics KK, Japan). When a designed holographic pattern is sent to the SLM as a Digital Visual Interface signal, the SLM functions as a Fourier phase hologram that generates seven focused laser spots in the focal plane of the objective,  $L_o$  (UPlanApo  $\times 60$ , numerical aperture = 1.20, water immersion, Olympus, Japan). An example of the holograms generated by the gratings and lens method [17–19] is shown in Fig. 1(b). In the gratings and lens method, the phase holograms of optical gratings, which deflect light to an arbitrary position as 1st-order diffraction light, are superimposed. In this system, the positions of the laser spots can be adjusted only by changing the hologram without any mechanical adjustment. The phase hologram is imaged in the back focal plane of  $L_o$  using a  $1 \times$  telescope consisting of  $L_1$  and  $L_2$ . The fluorescence spots excited by the beam-spot array are shown in Fig. 1(c). There were also undesired beam spots, 0th-order diffraction light, and 2nd- or higher-order diffraction light for each grating of hologram, outside of the field of view. Such undesired beam spots do not disturb the MP-hFCS measurement; however, they cause the loss of excitation light. The emitted fluorescence is focused on the seven optical fiber cores of a multicore fiber with a magnification of  $60 \times$  using the imaging lenses  $L_1$  and  $L_o$  (Fig. 1(d)). Each aperture of the fiber core functions as a pinhole (Fig. 1(e)), such that the fluorescence detection is equivalent to confocal detection in multiple channels. Any geometry of illuminated points can be realized via the SLM; however, the geometry of confocal detection points cannot be defined arbitrarily, because the measurement positions are defined by the positions corresponding to the fiber cores. The output signals from the PMT array are recorded with a time resolution of 1  $\mu$ s by a computer through a multichannel 8-bit pulse counting board, whose sampling rate is 80 MHz, constructed using the field-programmable gate array board used in a previous M-TIR-FCS system [11]. Autocorrelation functions (ACFs) and cross-correlation functions (CCFs) among the channels are calculated using newly developed software for the multichannel calculation of ACFs/CCFs. By fitting the FCS model equations to the ACFs, the

kinetics of fluorescent molecules (i.e., the diffusion times and the number of molecules) at the seven points can be determined simultaneously. The MP-hFCS system can perform multipoint FCS measurement at an arbitrary depth in three-dimensional samples because the multipoint confocal detection is realized via the holography technique and the multicore fiber. This is a significant advantage over M-TIR-FCS, where measurement can only be performed near the surface of the coverslip.

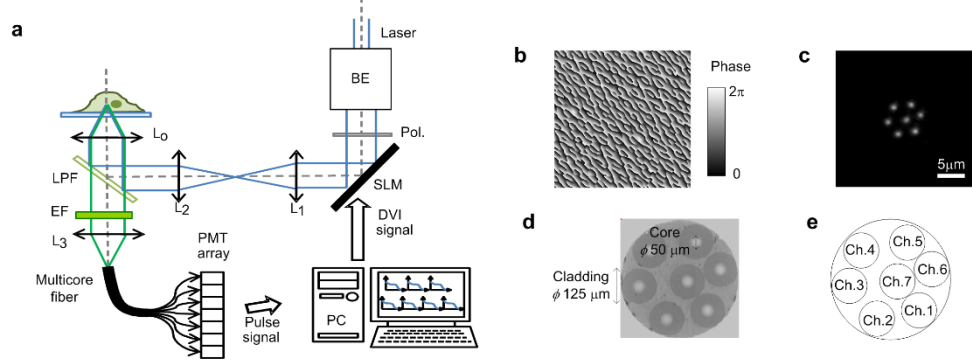


Fig. 1. Schematic of the experimental setup. (a) Optical settings. BE: beam expander. Lenses  $L_1$  and  $L_2$  constitute a  $1 \times$  telescope. The focal plane of the objective lens  $L_0$  is a Fourier plane of the SLM plane.  $L_0$  and  $L_3$  constitute a  $60 \times$  microscope, and the end terminal of the multicore fiber is an image plane of the focal plane of  $L_0$ . LPF is a long-path filter that reflects light with a wavelength longer than 495 nm, which passes through the LPF. EF: emission filter (transparent for light with wavelengths ranging from 520 to 535 nm). (b) Fourier phase hologram pattern that generates the fluorescence intensity distribution of a rhodamine 6G fluorophore adsorbed coverslip excited by the seven-beam spot array (c). (d) Microscopic image of the end terminal of the multicore fiber. (e) Schematic of the channel design.

## 2.2 FCS measurement and analysis

In all measurements, the ACFs or CCFs in the direction of channel  $n$  to  $m$  were calculated to analyze the fluorophore dynamics, as follows:

$$G_c^{n,m}(\tau) = \frac{\langle I_n(t) \cdot I_m(t + \tau) \rangle}{\bar{I}_n \cdot \bar{I}_m}, \quad (1)$$

where  $I_n$  and  $\bar{I}_n$  represent the fluorescence intensity signal of channel  $n$  and its time average, respectively. The bracket  $\langle \rangle$  represents the ensemble average operation. In the case of  $n = m$ , Eq. (1) is the ACF of channel  $n$ . Equation (1) also represents the spatiotemporal CCF. When there is a flow toward channel  $m$  from  $n$ , the spatiotemporal CCF  $G_c^{n,m}(\tau)$  has a peak at the traveling time to  $m$  from  $n$ .

If a fluorophore diffuses slowly, the diffusion time is long, and the decay rate of the ACF is low. A larger number of fluorescent molecules yields a lower amplitude of the ACF. Each ACF obtained by the MP-hFCS system was fitted with the theoretical ACF of FCS [21], as follows:

$$G_c^{n,n}(\tau) = 1 + \frac{1 - F_{\text{triplet}} + F_{\text{triplet}} \exp(-\tau / \tau_{\text{triplet}})}{N(1 - F_{\text{triplet}})} \cdot \sum_i \frac{F_i}{(1 + \tau / \tau_{Di}) \sqrt{1 + \tau / (s^2 \tau_{Di})}}, \quad (2)$$

where  $F_{\text{triplet}}$  and  $\tau_{\text{triplet}}$  are the average fraction of triplet-state molecules and the triplet relaxation time, respectively. The fraction and the diffusion time of the  $i^{\text{th}}$  component are expressed as  $F_i$  and  $\tau_{Di}$ , respectively.  $N$  is the number of fluorescent molecules in the detection volume defined by the radius  $w_0$  and length  $2z_0$ , and  $s$  is a structural parameter given by  $s = z_0/w_0$ . The normalized ACF is defined by

$$G_{\text{norm}}(\tau) = N(G(\tau) - 1). \quad (3)$$

The diffusion constant of the  $i^{\text{th}}$  component can be calculated using the equation  $D_i = w_0^2/4\tau_{Di}$ .  $w_0$  and  $s$  can be obtained via the measurement of a rhodamine 6G solution as a standard sample whose diffusion constant is  $414 \mu\text{m}^2/\text{s}$ . The detection volume  $V$  can be obtained as  $V = \pi^{3/2} w_0^2 z_0$ . The molar concentration  $C$  can be estimated as  $C = N/(V \cdot N_A)$ , where  $N_A$  is Avogadro's number.

### 2.3 FCS measurement and analysis in cells

The forward correlation to the nucleoplasm from the cytosol  $G_c^{c,n}(\tau)$  and the backward correlation  $G_c^{n,c}(\tau)$  are defined as

$$G_c^{c,n}(\tau) = \langle F_n(t, \mathbf{r}) F_c(t + \tau, \mathbf{r}') \rangle / \langle F_n \rangle \langle F_c \rangle, \quad (4)$$

$$G_c^{n,c}(\tau) = \langle F_c(t, \mathbf{r}') F_n(t + \tau, \mathbf{r}) \rangle / \langle F_n \rangle \langle F_c \rangle, \quad (5)$$

where  $F_n$  and  $F_c$  represent the fluctuating fluorescence intensity detected in the nucleus and the cytosol, respectively.  $\mathbf{r}$  and  $\mathbf{r}'$  are the positions of the measurement points in the nucleus and the cytosol, respectively. The brackets represent the time average operation. If there is molecular translocation to the nucleus from the cytosol, the forward correlation must have a peak corresponding to the traveling time between the two measurement points. Such an anisotropic component can be easily extracted by using the difference curve of these CCFs:  $G_c(\tau) = G_c^{c,n} - G_c^{n,c}$ .

### 2.4 Transient transfection in cell culture

HeLa cells were transfected using the Optifect Transfection Reagent (Invitrogen, USA) with  $0.5 \mu\text{L}/\text{well}$  green fluorescent protein (GFP) or GFP-GR $\alpha^{\text{wt}}$ , according to the instructions provided by the manufacturer.

## 3. Results

### 3.1 Experiments on aqueous solution

The shape of the confocal volume of the newly developed MP-hFCS system was first investigated via measurement of a rhodamine 6G water solution as a standard dye with a known diffusion coefficient ( $D = 414 \mu\text{m}^2/\text{s}$ ) [20]. The typical ACFs of rhodamine 6G measured by each channel are shown in Fig. 2(a). The ACFs of such a fast-diffusing dye were successfully measured because of the high time resolution of MP-hFCS, whereas it is difficult to measure such fast-diffusing dyes using other multipoint methods that sacrifice the temporal resolution. The diffusion times and structural parameters of each channel are shown in Figs. 2(b) and 2(c), respectively. All the fitted parameters are shown in [Data File 1](#). The average diffusion time and structural parameter of the seven channels were  $\tau_D = 70.3 \pm 3.5 \mu\text{s}$  and  $s = 4.88 \pm 0.21$ , respectively. Using the known diffusion coefficient of rhodamine 6G, the average waist and measurement volume of the seven channels were determined as  $w_0 = 339 \pm 9 \text{ nm}$  and  $V = 1.11 \pm 0.08 \text{ fL}$ , respectively (see the "FCS measurement and analysis" section). The waist of the confocal volume,  $w_0$ , was slightly larger than the diffraction limit ( $\sim 250 \text{ nm}$ ). The fiber core (1.67 airy unit), which acted as a pinhole, has a larger diameter than airy disc. To decrease the volume, a smaller fiber core or an objective lens with a higher magnification is needed. These data indicate that the MP-hFCS system had multiple confocal volumes with relatively uniform shapes.

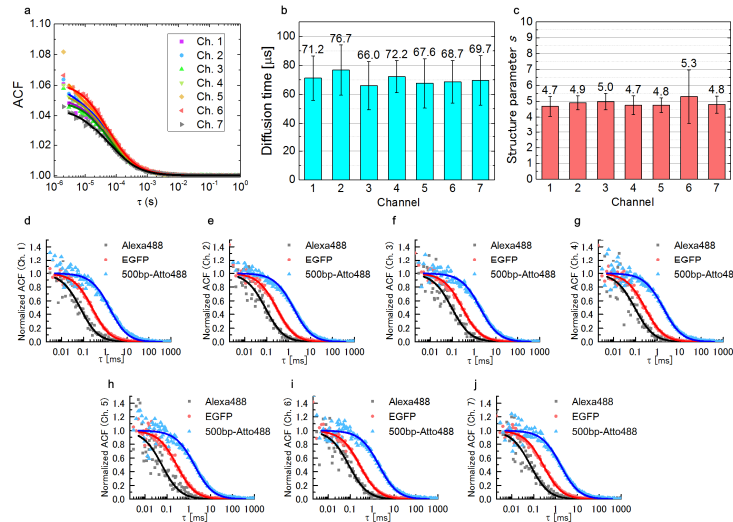


Fig. 2. System proof of concept. (a) Typical ACFs of a solution of rhodamine 6G measured using each channel of the MP-hFCS system. The symbols and solid lines show the experimental results and fitted curves, respectively. (b) Diffusion times measured by each channel. (c) Structural parameters measured by each channel. The error bars represent the standard deviations ( $n = 13$ ). (d)–(j) Normalized ACFs of each channel obtained simultaneously via MP-hFCS. The samples were aqueous solutions of Alexa 488 dye (0.6 kDa), GFP (27 kDa), and 500 base pairs of DNA labeled with Atto 488 dye (660 kDa). The symbols and solid lines represent the experimental results and fitted curves, respectively.

Measurements were performed for three different kinds of fluorescent molecules with widely differing molecular weights: an aqueous solution of Alexa Fluor 488 (0.6 kDa), a solution of GFP in PBS (27 kDa), and an aqueous solution of a 500-base pair DNA molecule labeled with Atto 488 (660 kDa). The resulting data are shown in Figs. 2(d)–2(j). The decay of the ACF became slower as the molecular weight increased, in accordance with diffusion theory. Table 1 presents a comparison of the diffusion coefficients and the count per molecule (CPM), which is the average fluorescence count rate (CR) per molecule, measured using MP-hFCS and a commercial FCS system (ConfoCor 2 unit built into LSM 510 Meta, ZEISS, Germany). All the fitted parameters are shown in [Data File 2](#). The data confirm that solutions of fluorescent molecules with various diffusion coefficients could be measured via MP-hFCS and that the results were similar to those of the other well-established system. The relatively large standard deviation of the diffusion coefficients obtained via MP-hFCS likely arose from the low laser power per measurement point due to the laser spot separation. This is supported by the low CPMs obtained via MP-hFCS. The low CPM was likely caused by a factor such as the narrow transparent band of the emission filter (520–535 nm for MP-hFCS and 505–550 nm for ConfoCor2), diffraction of an unwanted order, or fluorescence crosstalk. To reduce the standard deviation of the diffusion coefficient, either the laser power or the measurement duration can be increased.

**Table 1. Comparison of MP-hFCS and ConfoCor3 analysis of the different dye solutions.**

Sample	$D$ [ $\mu\text{m}^2/\text{s}$ ]		CPM [kHz]	
	MP-hFCS	ConfoCor 3	MP-hFCS	ConfoCor 3
Alexa 488	$378.3 \pm 79.7$	$358.6 \pm 11.8$	$0.68 \pm 0.13$	$22.08 \pm 0.50$
GFP	$109.2 \pm 21.8$	$126.0 \pm 3.6$	$1.08 \pm 0.24$	$22.09 \pm 0.08$
500 bp DNA	$16.8 \pm 3.6$	$12.0 \pm 0.6$	$0.55 \pm 0.13$	$10.19 \pm 0.26$

Data are the mean  $\pm$  standard deviation. The MP-hFCS data are the average value of seven channels, with one measurement each ( $n = 7$ ). The ConfoCor 3 data are the average value of three independent measurements ( $n = 3$ ).

### 3.2 Experiments on living cell

MP-hFCS measurements were performed on a single HeLa cell transiently expressing GFP, as shown in Fig. 3(a). Channels 1 and 7 were in the nucleolus, and the remaining channels were in the nucleoplasm. As shown in Fig. 3(b), the height of the boundary between the coverslip and the cell was defined as  $z = 0 \mu\text{m}$ . The upper direction was defined as the positive direction of the  $z$ -axis. MP-hFCS measurements were performed from  $z = -1$  to  $8 \mu\text{m}$  at intervals of  $1 \mu\text{m}$ . The fluorescence photon CR distribution, which corresponds to the fluorescence intensity, is shown in Fig. 3(c). The CRs inside the nucleolus were lower than those inside the nucleoplasm. This result is in good agreement with a previous study [22] and might be due to the dense fibrillar component in the nucleolus. In addition, each CR distribution had single peak at  $z = 4 \mu\text{m}$ , which was attributed to the center plane of the cell. The normalized ACFs of channel 1 (nucleolus) and channel 4 (nucleoplasm) measured at  $z = 4 \mu\text{m}$  are shown in Fig. 3(d).

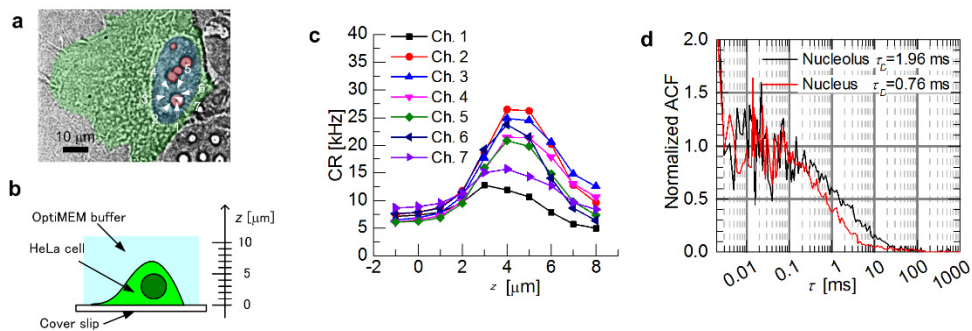


Fig. 3. *In vivo* MP-hFCS measurements of a HeLa cell transiently expressing GFP. (a) Bright-field image of the HeLa cell. The white arrows indicate the measurement positions. The cytosol, nucleus, and nucleolus are digitally colored green, blue, and red, respectively. The image contrast was enhanced by image processing. (b) Schematic and definition of the  $z$ -axis. (c) CRs with respect to  $z$ . (d) ACFs in the nucleolus and the nucleus. The excitation laser power was approximately  $2.5 \mu\text{W}$  per channel, and the measurements were performed five times for each 5 s. The diffusion times of the GFP in the nucleolus and nucleoplasm were obtained by fitting a single-component model to the ACF, and they were  $\tau_D = 1.96$  and  $0.76$ , respectively.

The wild-type human glucocorticoid receptor  $\alpha$  ( $\text{GR}\alpha^{\text{wt}}$ ) is a nuclear receptor localized in the cytosol in the absence of a ligand. Following the binding of a ligand such as dexamethasone (Dex),  $\text{GR}\alpha^{\text{wt}}$  translocates to the nucleus through the nuclear pore complex (NPC). Finally,  $\text{GR}\alpha^{\text{wt}}$  binds to DNA and regulates the expression of its target genes. The transition time of  $\text{GR}\alpha^{\text{wt}}$  through the NPC, which has remained unclear, was analyzed as one of the applications of MP-hFCS. Figures 4(a) and 4(b) show HeLa cells transiently expressing GFP and GFP- $\text{GR}\alpha^{\text{wt}}$ , respectively. The measurement points (white arrows) were reduced to two in order to reduce the phototoxicity for this long-term measurement. Figures 4(c) and 4(d) show the CRs of GFP and GFP- $\text{GR}\alpha^{\text{wt}}$ , respectively. For this measurement, 100 nM Dex (final concentration)—a  $\text{GR}\alpha^{\text{wt}}$  ligand—was added to the cell culture medium at 0 s. The CRs of the GFP in both the nucleoplasm and the cytosol remained unchanged. In contrast, following Dex treatment, the CR of the GFP- $\text{GR}\alpha^{\text{wt}}$  in the cytosol decreased, and that in the nucleoplasm increased. These results confirm the nuclear translocation of GFP- $\text{GR}\alpha^{\text{wt}}$  after Dex addition. The 10-s measurement was repeated 54 times. For each time course measurement, 18 measurements were concatenated, and the ACFs were calculated. Finally, we obtained three ACFs for the time regions of  $-180$  to  $0$ ,  $0$  to  $180$ , and  $180$  to  $360$  s. The time lag between each 10-s measurement was negligible. Figures 4(e)–4(h) show the ACFs, and the fitted results obtained using either a single- or double-component model (see the

“FCS measurement and analysis” section) are shown in [Data File 3](#). Figures 4(e) and 4(g) show the ACFs of the GFP in the cytosol and the nucleoplasm, respectively, and Figs. 4(f) and 4(h) show those of the GFP-GR $\alpha^{wt}$ . In the case of the GFP, the number of fluorescent molecules ( $N$ ) and the diffusion time ( $\tau_{D1}$ ) remained unchanged in the nucleoplasm and the cytosol following Dex treatment. Whereas the  $N$  in the nucleoplasm was increased by adding Dex, the  $N$  in the cytosol decreased. In addition, the diffusion constants  $D_1$  and  $D_2$  in the nucleus decreased, and the fraction of the slow component increased. These results agree well with the FCS results from a previous report [23], which concluded that GFP-GR $\alpha^{wt}$  was bound to the DNA inside the nucleus. The ACF in the nucleoplasm during the period of  $-180$  to  $0$  s could not be calculated, because of the very small amount of GFP-GR $\alpha^{wt}$  present in the nucleus prior to Dex addition. The mean diffusion constants and diffusion times of the GFP and GFP-GR $\alpha^{wt}$  calculated for several different cells of the same cell line (HeLa) are shown in [Data File 4](#).

MP-hFCS measurement also provides the spatiotemporal CCF, whereby the average transition time of each molecular flow can be obtained from the same signals used in the ACF analysis [8]. The forward correlation to the nucleoplasm from the cytosol  $G_c^{c,n}(\tau)$ , the backward correlation  $G_c^{n,c}(\tau)$ , and the difference curve  $G_c(\tau)$  defined by Eqs. (4) and (5) were used. If there is a molecular flow,  $G_c(\tau)$  should have a peak at  $\tau$  corresponding to the flow rate because two measurement channels detect similar fluorescence intensity signals with a time difference according to the transition time between the two channels.

Figures 4(i) and 4(j) show the  $G_c(\tau)$  of the GFP and GFP-GR $\alpha^{wt}$ , respectively. The  $G_c$  of the GFP had no peaks, indicating that the diffusion of the GFP (27 kDa) was non-directional because molecules smaller than 40 kDa could freely pass through the NPC via free diffusion. In contrast, peaks appeared on the  $G_c$  for the GFP-GR $\alpha^{wt}$  (113 kDa) after the addition of Dex. This result shows that the GFP-GR $\alpha^{wt}$  molecule was unidirectionally translocated to the nucleus via active transport. The peaks were at  $\tau \approx 45.1$  s; therefore, the nuclear translocation of GFP-GR $\alpha^{wt}$  between two measurement points took 45.1 s. If there is no membrane and GFP-GR $\alpha^{wt}$  diffuses freely between the two measurement points, a peak should appear at 149.0 ms. The latter time was calculated by assuming a mean diffusion constant of  $6.43 \mu\text{m}^2/\text{s}$  for GFP-GR $\alpha^{wt}$  in cytosol, using the CCFs based on the dual-focus FCS theorem [8]. Interestingly, the measured GFP-GR $\alpha^{wt}$  nuclear translocation time was significantly longer (more than 300-fold) than the expected result for free diffusion. In addition, it was far longer than that observed for NLS-GFP (27 kDa) translocation via the nuclear membrane, which ranged from 1 to 40 ms [24]. This large difference in the transition time could be due to the large molecular size of GFP-GR $\alpha^{wt}$ , as large molecules have difficulty passing through the holes of NPCs. These data therefore suggest that there could be a relationship among the transition time, molecular size, and energy expense.

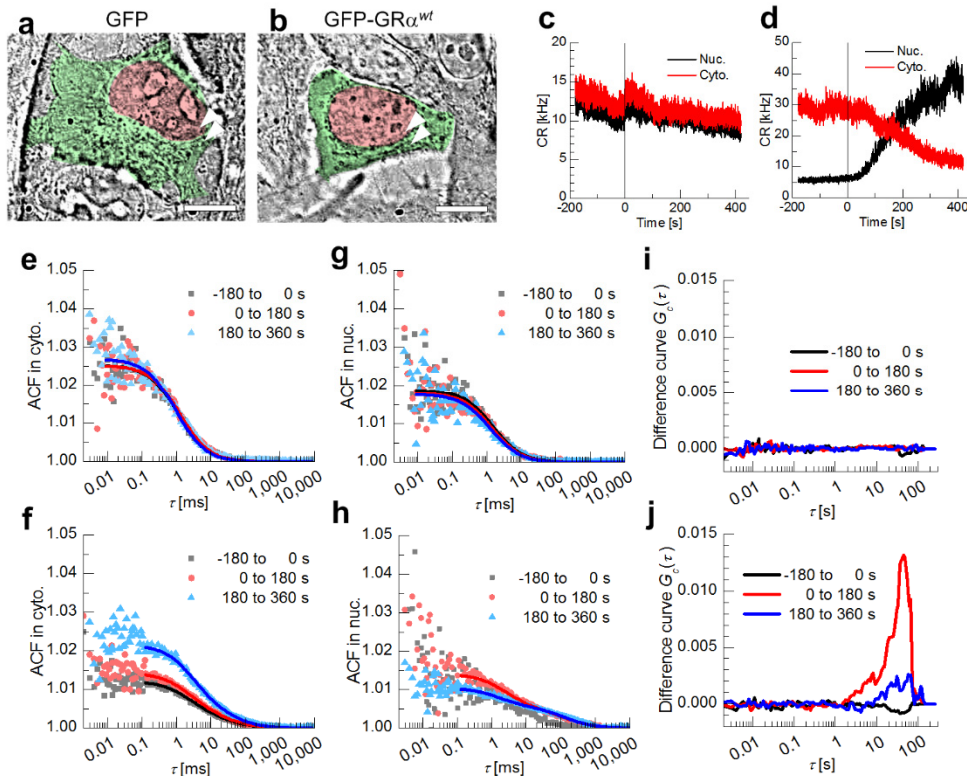


Fig. 4. ACFs and spatiotemporal CCFs for the *in vivo* MP-hFCS measurement of HeLa cells transiently expressing GFP or GFP-GR $\alpha^{wt}$ . Panels (a), (c), (e), and (g) show HeLa cells expressing GFP. The fluctuation of the CR at 0 s was caused by the impact of adding the Dex solution in (c). Panels (b), (d), (f), and (h) show HeLa cells expressing GFP-GR $\alpha^{wt}$ . (a, b) Bright-field images of HeLa cells. The white arrows indicate the measurement positions. The two measurement points indicated are channels 5 and 6, and the distance between them was 2.3  $\mu\text{m}$ . The cytosol and the nucleus are digitally colored green and red, respectively, and the contrast was enhanced by image processing. The scale bar represents 10  $\mu\text{m}$ . (c, d) CRs with respect to time. 100 nM Dex was added at 0 s. (e, f) ACFs in the cytosol. (g, h) ACFs in the nucleus. (i, j) Difference curves of  $G_c(\tau)$  for HeLa cells expressing GFP and for HeLa cells expressing GFP-GR $\alpha^{wt}$ . Note the absence of peaks in (i) and the presence of a single peak in (j) at  $t = 45.1$  s. The laser power was approximately 2.5  $\mu\text{W}$  per channel, and measurements were performed 60 times for each 10 s.

#### 4. Conclusions

We described the development of a new MP-hFCS system based on flexible wavefront control optics and confocal detection. Because of this highly flexible illumination [18], we can realize any pattern of multiple confocal detection with other multicore fibers. In this MP-hFCS system, one PMT and one counter were used for each channel while both the photon sensitivity and the time resolution were maintained. It was demonstrated that the confocal volumes of the MP-hFCS could be determined using organic fluorescent dyes; such measurement is difficult using other multipoint methods that sacrifice the time resolution. The MP-hFCS system was used *in vivo* to detect GFP inside a HeLa cell. The dynamics of the GFP diffusion were measured simultaneously at seven points. Introducing spatiotemporal CCF analysis to the MP-hFCS system allowed for the calculation of the transition time for nuclear transport through the nuclear membrane of Dex-bound GFP-GR $\alpha^{wt}$  which was found to be approximately 45.1 s. Although this transition time was significantly shorter than

expected and this issue remains to be resolved, the proposed MP-hFCS system is capable of detecting directional molecular diffusion.

We anticipate that the MP-hFCS system will be useful for revealing various properties of molecular dynamics, such as flow, translocation, and intracellular communication. We also believe that by using faster detectors with less noise [25,26], the MP-hFCS measurement can be extended to a faster correlation time for obtaining rotational diffusion coefficients that are more approximate to the molecular shape and orientation of oligomerization than current MP-hFCS system.

## Funding

Grant-in-Aid for Scientific Research (JSPS KAKENHI) (S) (JP21221006) and Grant-in-Aid for Scientific Research (JSPS KAKENHI) (C) (JP16K07312).

## Disclosures

The authors declare that there are no conflicts of interest related to this article.

## References

1. E. L. Elson and D. Magde, "Fluorescence correlation spectroscopy. I. Conceptual basis and theory," *Biopolymers* **13**(1), 1–27 (1974).
2. R. Rigler, Ü. Mets, J. Widengren, and P. Kask, "Fluorescence correlation spectroscopy with high count rate and low background: analysis of translational diffusion," *Eur. Biophys. J.* **22**(3), 169–175 (1993).
3. C. G. Pack, G. Nishimura, M. Tamura, K. Aoki, H. Taguchi, M. Yoshida, and M. Kinjo, "Analysis of interaction between chaperonin GroEL and its substrate using fluorescence correlation spectroscopy," *Cytometry* **36**(3), 247–253 (1999).
4. R. T. Kovacic and K. E. van Holde, "Sedimentation of homogeneous double-strand DNA molecules," *Biochemistry* **16**(7), 1490–1498 (1977).
5. S. Björling, M. Kinjo, Z. Földes-Papp, E. Hagman, P. Thyberg, and R. Rigler, "Fluorescence correlation spectroscopy of enzymatic DNA polymerization," *Biochemistry* **37**(37), 12971–12978 (1998).
6. S. Oasa, A. Sasaki, J. Yamamoto, S. Mikuni, and M. Kinjo, "Homodimerization of glucocorticoid receptor from single cells investigated using fluorescence correlation spectroscopy and microwells," *FEBS Lett.* **589**(17), 2171–2178 (2015).
7. M. Kinjo and R. Rigler, "Ultrasensitive hybridization analysis using fluorescence correlation spectroscopy," *Nucleic Acids Res.* **23**(10), 1795–1799 (1995).
8. M. Brinkmeier, K. Dörre, J. Stephan, and M. Eigen, "Two-beam cross-correlation: a method to characterize transport phenomena in micrometer-sized structures," *Anal. Chem.* **71**(3), 609–616 (1999).
9. A. P. Singh, J. W. Krieger, J. Buchholz, E. Charbon, J. Langowski, and T. Wohland, "The performance of 2D array detectors for light sheet based fluorescence correlation spectroscopy," *Opt. Express* **21**(7), 8652–8668 (2013).
10. D. K. Papadopoulos, A. J. Krmpot, S. N. Nikolić, R. Krautz, L. Terenius, P. Tomancak, R. Rigler, W. J. Gehring, and V. Vukojević, "Probing the kinetic landscape of Hox transcription factor-DNA binding in live cells by massively parallel Fluorescence Correlation Spectroscopy," *Mech. Dev.* **138**(Pt 2), 218–225 (2015).
11. Y. Ohsugi and M. Kinjo, "Multipoint fluorescence correlation spectroscopy with total internal reflection fluorescence microscope," *J. Biomed. Opt.* **14**(1), 014030 (2009).
12. P. W. Wiseman, J. A. Squier, M. H. Ellisman, and K. R. Wilson, "Two-photon image correlation spectroscopy and image cross-correlation spectroscopy," *J. Microsc.* **200**(1), 14–25 (2000).
13. B. Kannan, J. Y. Har, P. Liu, I. Maruyama, A. Jeak Ling Ding, and Thorsten Wohland, "Electron Multiplying Charge-Coupled Device Camera Based Fluorescence Correlation Spectroscopy," (2006).
14. F. Cardarelli and E. Gratton, "In vivo imaging of single-molecule translocation through nuclear pore complexes by pair correlation functions," *PLoS One* **5**(5), e10475 (2010).
15. M. A. Digman, P. Sengupta, P. W. Wiseman, C. M. Brown, A. R. Horwitz, and E. Gratton, "Fluctuation Correlation Spectroscopy with a Laser-Scanning Microscope: Exploiting the Hidden Time Structure," *Biophys. J.* **88**(5), L33–L36 (2005).
16. T. Wohland, J. Sankaran, M. Manna, and R. S. Kraut, "Imaging Total Internal Reflection Fluorescence Correlation Spectroscopy (ITIR-FCS) Detects Multiple Lipid Domains on Live Cell Membranes," *Biophys. J.* **100**(3), 475 (2011).
17. J. Liesener, M. Reichert, T. Haist, and H. J. Tiziani, "Multi-Functional Optical Tweezers Using Computer-Generated Holograms," *Opt. Commun.* **185**(1), 77–82 (2000).
18. J. Leach, K. Wulff, G. Sinclair, P. Jordan, J. Courtial, L. Thomson, G. Gibson, K. Karunwi, J. Cooper, Z. J. Laczik, and M. Padgett, "Interactive approach to optical tweezers control," *Appl. Opt.* **45**(5), 897–903 (2006).
19. J. Yamamoto and T. Iwai, "Highly Controllable Optical Tweezers Using Dynamic Electronic Holograms," *Curr. Pharm. Biotechnol.* **13**(14), 2655–2662 (2012).

20. C. B. Müller, A. Loman, V. Pacheco, F. Koberling, D. Willbold, W. Richtering, and J. Enderlein, "Precise measurement of diffusion by multi-color dual-focus fluorescence correlation spectroscopy," *EPL (Europhysics Lett.)* **83**(4), 46001 (2008).
21. J. R. Lakowicz, *Principles of Fluorescence Spectroscopy*, 3rd ed. (Springer US, 2006).
22. C. Pack, K. Saito, M. Tamura, and M. Kinjo, "Microenvironment and Effect of Energy Depletion in the Nucleus Analyzed by Mobility of Multiple Oligomeric EGFPs," *Biophys. J.* **91**(10), 3921–3936 (2006).
23. S. Mikuni, M. Tamura, and M. Kinjo, "Analysis of intranuclear binding process of glucocorticoid receptor using fluorescence correlation spectroscopy," *FEBS Lett.* **581**(3), 389–393 (2007).
24. U. Kubitscheck, D. Grünwald, A. Hoekstra, D. Rohleder, T. Kues, J. P. Siebrasse, and R. Peters, "Nuclear transport of single molecules: dwell times at the nuclear pore complex," *J. Cell Biol.* **168**(2), 233–243 (2005).
25. J. Yamamoto, M. Oura, T. Yamashita, S. Miki, T. Jin, T. Haraguchi, Y. Hiraoka, H. Terai, and M. Kinjo, "Rotational diffusion measurements using polarization-dependent fluorescence correlation spectroscopy based on superconducting nanowire single-photon detector," *Opt. Express* **23**(25), 32633–32642 (2015).
26. M. Oura, J. Yamamoto, H. Ishikawa, S. Mikuni, R. Fukushima, and M. Kinjo, "Polarization-dependent fluorescence correlation spectroscopy for studying structural properties of proteins in living cell," *Sci. Rep.* **6**(1), 31091 (2016).